## JBC ARTICLE

updates

# *In vivo* crystals reveal critical features of the interaction between cystic fibrosis transmembrane conductance regulator (CFTR) and the PDZ2 domain of Na⁺/H⁺ exchange cofactor NHERF1

 Eleanor R. Martin[‡§1],  Alessandro Barbieri[‡¶],  Robert C. Ford[‡], and  Robert C. Robinson[§‖**2]

From the ‡School of Biological Sciences, Faculty of Biology Medicine and Health, Michael Smith Building, The University of Manchester, Manchester M13 9PL, United Kingdom, the §Institute of Molecular and Cell Biology, A*STAR (Agency for Science, Technology and Research), Biopolis 138673, Singapore, the ¶Bioinformatics Institute (BII), A*STAR (Agency for Science, Technology and Research), Biopolis 138671, Singapore, the ‖School of Biomolecular Science and Engineering (BSE), Vidyasirimedhi Institute of Science and Technology (VISTEC), Rayong 21210, Thailand, and the **Research Institute for Interdisciplinary Science, Okayama University, Okayama 700-8530, Japan

Edited by Joseph M. Jez

Crystallization of recombinant proteins has been fundamental to our understanding of protein function, dysfunction, and molecular recognition. However, this information has often been gleaned under extremely nonphysiological protein, salt, and H⁺ concentrations. Here, we describe the development of a robust Inka1-Box (iBox)–PAK4cat system that spontaneously crystallizes in several mammalian cell types. The semi-quantitative assay described here allows the measurement of *in vivo* protein-protein interactions using a novel GFP-linked reporter system that produces fluorescent readouts from protein crystals. We combined this assay with *in vitro* X-ray crystallography and molecular dynamics studies to characterize the molecular determinants of the interaction between the PDZ2 domain of Na⁺/H⁺ exchange regulatory cofactor NHE-RF1 (NHERF1) and cystic fibrosis transmembrane conductance regulator (CFTR), a protein complex pertinent to the genetic disease cystic fibrosis. These experiments revealed the crystal structure of the extended PDZ domain of NHERF1 and indicated, contrary to what has been previously reported, that residue selection at positions −1 and −3 of the PDZ-binding motif influences the affinity and specificity of the NHERF1 PDZ2-CFTR interaction. Our results suggest that this system could be utilized to screen additional protein-protein interactions, provided they can be accommodated within the spacious iBox-PAK4cat lattice.

The catalytic domain of the serine/threonine kinase PAK4 (PAK4cat)[3] and its endogenous inhibitor Inka1 have recently been shown to readily form rod-type crystals on co-transfection into a variety of mammalian cell types (1). Crystals formed following transfection of a fusion construct comprised of a central 38-residue region of Inka1, termed the Inka1-Box (iBox), and PAK4cat (iBox-PAK4cat) were diffracted at the synchrotron beamline, enabling the first *in cellulo* human protein structure to be determined to 2.95 Å (PDB 4XBR). The crystal lattice revealed that iBox-PAK4cat forms a hexagonal array with channels 80 Å in diameter that run the length of the crystal. The size of this cavity allowed a guest protein (GFP) to be incorporated into the crystal lattice (1). This, as well as the relative ease with which crystals can be generated following transfection of DNA into mammalian cells, suggests that iBox-PAK4cat crystals may be a useful tool for a variety of experimental purposes, including crystallization of guest proteins, use as environmentally responsive cellular sensors, and use in protein-protein interaction (PPI) screening assays. However, the potential uses of iBox-PAK4cat *in cellulo* crystals for both structural and other applications, are relatively unexplored and require further study.

PSD-95/Dlg-1/ZO-1 (PDZ) domains constitute one of the most commonly identified protein interaction modules, with over 500 PDZ domain-containing proteins identified in the human genome alone (2). PDZ domains characterized to date share a common core structure, consisting of a 6-stranded antiparallel β sandwich structure (β1–β6) flanked by an α helix on each side (α1, α2). PDZ domains fulfil their scaffolding function through the recognition of short linear PDZ-binding motifs that are commonly found at the extreme C termini of receptors and ion channels. It is generally agreed that PDZ-

binding motifs are comprised of four residues, referred to by convention as P0, P-1, P-2, and P-3 from the C-terminal residue inward. Early studies characterizing PDZ domain-motif interactions led to the classification of PDZ domains based on their preferences for particular PDZ-binding motifs, indicating motif selection is primarily dictated by the motif residues at P0 and P-2. Peptide library screening studies identified PDZ domains that displayed distinct preferences for the type I motif $X$-(S/T)-$X$-$\Phi$ (where $\Phi$ is a hydrophobic amino acid and $X$ is any amino acid), the type II motif $X$-$\Phi$-$X$-$\Phi$ (3, 4), or the less common type III motif $X$-(D/E)-$X$-$\Phi$ (5).

The cystic fibrosis transmembrane conductance regulator (CFTR), or ABCC7, is a chloride ion channel expressed in the epithelia of the airways, intestine, pancreas, sweat gland, and testis (6). Loss-of-function mutations of CFTR cause the autosomal-recessive disease cystic fibrosis (CF). CF is the most prevalent genetic disease among European populations, affecting on average 1 in every 3500 live births (7). The most common CF-causing mutation is the deletion of phenylalanine at position 508 (F508del), which is present on at least one allele in 90% of patients in some populations (8). The F508del mutation causes protein misfolding and subsequent targeting of CFTR for degradation via the endoplasmic reticulum-associated degradation pathway (9). CFTR contains the conserved type I PDZ-binding motif (D/E)T(R/K)L at its C terminus. Through this motif, CFTR is known to interact with several PDZ domain-containing proteins, including CFTR-associated ligand (CAL), Shank2, as well as all four members of the NHERF family (NHERF1, NHERF2, NHERF3, and NHERF4) (10–13). NHERF1 is comprised of two PDZ domains (PDZ1 and PDZ2), both of which are able to bind to the PDZ-binding motif of CFTR (10, 14–17). NHERF1 has been shown to increase both the activity and plasma membrane localization of both WT and F508del CFTR (18–23). Although mutations of the CFTR C terminus are rare, they have been reported as being disease-causing (24). Furthermore, CFTR variants in which the CFTR PDZ-binding motif is compromised through either truncation or substitution (*e.g.* S1455X, Q1476X, and L1480P) have been associated with various CF-related disorders such as elevated sweat chloride concentration and congenital bilateral absence of the vas deferens (see RRID:SCR_000685). It has been demonstrated that whereas F508del CFTR interacts poorly with NHERF1, the CFTR corrector VX-809 increases the binding affinity between these two proteins (25). Together, these studies suggest that one potential strategy for the further development of CF therapeutics may be the generation of small molecule corrector-type drugs specifically targeted at enhancing the interaction between NHERF1 and CFTR. Indeed, more generally, there is significant interest in targeting specific PDZ domain-motif interactions with small molecule inhibitors or peptides that block the PDZ-binding site (26, 27). The development of drugs that target certain PDZ domains but not others, however, remains challenging and requires further characterization of the molecular determinants of specific PDZ domain-motif interactions.

The experiments described here employ a variety of approaches to further characterize the molecular determinants of the interaction between the second PDZ domain of NHERF1

and the CFTR. These results indicate that the PDZ-binding motif of CFTR appears to be an optimal PDZ-binding motif for interaction with PDZ2 of NHERF1, and that residue selection at the −1 and −3 motif positions appears to influence the affinity and specificity of the interaction. These findings have been corroborated *in cellulo* through the development of a novel PPI screening assay based on the iBox-PAK4cat crystallization system. This study demonstrates that iBox-PAK4cat crystals represent a potentially useful tool for the study of PDZ domain-motif interactions in a cellular context and may be a useful tool in future screening studies.

## Results

### The structure of the extended NHERF1 PDZ2 domain

To understand fully the determinants of the NHERF1 PDZ2-CFTR interaction we sought to determine the co-crystal structure. To facilitate co-crystallization, a chimeric construct was generated in which the NHERF1 PDZ2 domain (NHERF1 residues 150–270) was fused to a C-terminal DTRL tetrapeptide motif corresponding to the last four residues of CFTR (CFTR residues 1477–1480), mirroring an approach commonly used for crystallization of PDZ domain-motif complexes (28–31). This strategy produced diffraction-quality crystals, enabling the structure to be solved and refined to 2.2 Å (Table 1).

The overall topology of the canonical NHERF1 PDZ2 domain is consistent with standard PDZ domains, comprising of a 6-stranded $\beta$-barrel ($\beta$1–$\beta$6) and two $\alpha$-helices ($\alpha$1 and $\alpha$2) (Fig. 1*A*). In agreement with previous reports (17), the structure revealed that NHERF1 PDZ2 contains additional structured extensions beyond the core PDZ-fold. These extended regions form an $\alpha$- ($\alpha$3) and a $3_{10}$ ($\alpha$4) helix, which pack against the $\beta$1, $\beta$4, and $\beta$6 strands through the formation of a closed hydrophobic cluster (Fig. 1*B*). Although this hydrophobic cluster is formed from residues distal to the binding site, the extended NHERF1 PDZ2 domain has been shown to have an almost 18-fold higher binding affinity for the CFTR C terminus than the canonical domain (17). Comparison of the structure of the extended NHERF1 PDZ2 with the canonical domain (NHERF1 residues 148–239) in the apo form (PDB 2OZF) reveals high structural similarity, with a RMSD of 0.74 Å for the 85 eq C$\alpha$ atoms (Fig. S1). This indicates that the extended region does not induce significant structural changes in the core PDZ domain, but rather conveys its effects through allosteric interactions that mediate the stability of the binding site. Interestingly, multiple sequence alignment and secondary structure predictions indicate that similar structured extensions outside of the core PDZ-fold are common to several members of the NHERF family (Fig. 3*B*, Fig. S2), although thus far only those of NHERF1 have been characterized.

### The determinants of the NHERF1 PDZ2-CFTR interaction

The PDZ-binding motif of CFTR inserts into the $\beta$2–$\alpha$2 binding groove in a canonical fashion (Figs. 1*A* and 2*A*), extending the $\beta$-sheet of the PDZ domain and burying a solvent-accessible surface area of 876 Å$^2$. The DTRL peptide at the CFTR C terminus represents a typical type I PDZ-binding motif, and

ŠASBMB

*J. Biol. Chem.* (2020) 295(14) 4464–4476 **4465**

**Table 1**
**Data collection and refinement statistics for the NHERF1 PDZ2-CFTR complex**

| Data collection | |
|---|---|
| Space group | $I2_12_12_1$ |
| Cell dimensions | |
| $a$, $b$, $c$ (Å) | 84.9, 85.0, 89.6 |
| $\alpha$, $\beta$, $\gamma$ (°) | 90.0, 90.0, 90.0 |
| Resolution (Å) | 19.8–2.20 (2.28–2.20) |
| $R_{merge}$ (%) | 17.6 (95.1) |
| $R_{pim}$ (%) | 11.3 (60.0) |
| $CC_{1/2}$ | 0.984 (0.634) |
| $I/\sigma(I)$ | 4.3 (1.6) |
| Unique reflections | 16,795 (1653) |
| Completeness (%) | 99.6 (97.8) |
| Multiplicity | 3.5 (3.6) |
| | |
| Refinement | |
| Resolution (Å) | 19.8–2.20 (2.35–2.20) |
| No. of reflections: working/test | 16,735/783 (2566/124) |
| $R_{work}$ / $R_{free}$ | 20.6/23.3 (28.6/32.1) |
| No. of atoms | 2,138 |
| Protein | 1,934 |
| Water | 204 |
| Average B-factor (Å²) | 39.3 |
| Protein (Å²) | 40.0 |
| Water (Å²) | 32.9 |
| RMSD | |
| Bond lengths (Å) | 0.004 |
| Bond angles (Å) | 0.913 |
| Ramachandran | |
| Favored (%) | 98.0 |
| Allowed (%) | 2.0 |
| Disallowed (%) | 0.0 |

as such, the structure presented here shares many common features with a typical type I PDZ domain-motif interaction. The T-2 residue of the PDZ-binding motif can be observed to form a hydrogen bond with a conserved histidine residue at position 212 of NHERF1 PDZ2 (Fig. 2*A*), consistent with a shared mechanism of recognition found in type I interactions. The L0 carboxyl group and leucine side chain appear to be key determinants of binding through interactions with the conserved $^{163}$GYGF$^{167}$ carboxylate-binding motif and hydrophobic binding pocket, respectively (Fig. 2). In particular, the binding pocket appears to be stereochemically adapted to accommodate the leucine side chain (Fig. 2*B*). Other residues of the PDZ-binding motif can be observed to take part in numerous interactions with the NHERF1 PDZ2 domain. Specifically, the D-3 side chain forms a salt bridge with Arg$^{180}$ and a hydrogen bond with His$^{169}$, and R-1 forms a salt bridge with Asp$^{183}$ and a hydrogen bond with Asn$^{167}$ (Fig. 2*A*).

Several studies have indicated that the CFTR C terminus binds to NHERF1 PDZ2 with lower affinity than PDZ1 (10, 17, 32). Indeed, whereas NHERF1 PDZ1 and PDZ2 domains share 54.4% sequence identity, they have been shown to display distinct differences with regards to ligand binding selectivity and affinity. The PDZ domains of NHERF1 are highly structurally similar (Fig. 3*A*). However, natural sequence variation of a number of key residues within the binding pocket can be observed, including the substitution of Glu-43 within PDZ1 with an aspartate residue at the equivalent position (Asp$^{183}$) within PDZ2 (Fig. 3*B*). Studies have suggested that the lower binding affinity of PDZ2 can be attributed to the shorter side chain of Asp$^{183}$ that cannot form a salt bridge with the R-1 residue of the CFTR PDZ-binding motif (17, 33). The crystal structure presented here contradicts this hypothesis, because

the salt bridge between Asp$^{183}$ and R-1 is present (Figs. 2*A* and 3*A*). The majority of known CFTR-binding PDZ domains contain a negatively charged residue at this position within the binding pocket, including those outside of the NHERF family such as Shank1 (Fig. 3*B*), implying that it is charge rather than side chain length that is important. Furthermore, a positively charged residue at P-1 of the PDZ-binding motif is conserved cross-species for CFTR (Fig. S3). As such, these results indicate that the formation of an ionic interaction between these two residues may be a common mechanism for recognition and selectivity between CFTR and its respective CFTR-binding PDZ domains.

### Use of iBox-PAK4cat in cellulo crystals as a tool for studying protein-protein interactions

The *in cellulo* crystal structure of iBox-PAK4cat revealed a hexagonal lattice with channels ~80 Å in diameter that run the length of the crystal (1). We hypothesized that it may be possible to introduce NHERF1 PDZ2 into the crystal lattice to facilitate its *in cellulo* crystallization. A NHERF1 PDZ2 containing iBox-PAK4cat fusion construct (iBox-PDZ2-PAK4cat) readily formed diffraction-quality crystals (Fig. S4, Table S1). A partial electron density map was revealed for the PDZ2 domain, although it was of insufficient quality to trace the full polypeptide chain (Fig. S5), indicating that additional construct optimization is required to stabilize guest proteins in a single orientation within the crystal lattice. GFP-containing fluorescent crystals have also been produced through co-transfection of PAK4cat with various GFP-Inka1 constructs (1). In an extension of these approaches, we postulated that, through monitoring of GFP fluorescence levels, iBox-PAK4cat crystals could also be utilized as high-density *in vivo* sensors for the detection of protein-protein interactions. In particular, we sought to utilize the iBox-PAK4cat system as a tool to enable detection of PDZ domain-motif interactions. This approach is summarized in Fig. 4*A*. Two crystal-forming constructs were tested, one containing a C-terminal tetrapeptide corresponding to the CFTR PDZ-binding motif (iBox-PAK4cat-DTRL), and a negative control containing a non PDZ-binding C-terminal motif (iBox-PAK4cat-AAAA). Although both iBox-PAK4cat-DTRL and iBox-PAK4cat-AAAA constructs appeared to be similar in terms of crystal generation proficiency (Fig. S6), iBox-PAK4cat-DTRL crystals demonstrated clearly observable GFP fluorescence on co-transfection with GFP-NHERF1PDZ1. Co-transfection with iBox-PAK4cat-AAAA, however, resulted in only cytoplasmic GFP fluorescence, with minimal fluorescence observable in the crystals (Fig. 4*B*). The easily visible crystals formed from GFP-NHERF1PDZ and iBox-PAK4cat-DTRL co-transfection allowed for time-lapse analysis of crystal formation (Movie S1).

### iBox-PAK4cat in cellulo protein-protein interaction assay reveals the determinants of NHERF1 PDZ domain binding selectivity

Because iBox-PAK4cat crystals enable clear visual differentiation between binding and nonbinding events on co-transfection with GFP-PDZ (Fig. 4*B*), we sought to determine whether this system could also detect changes to the
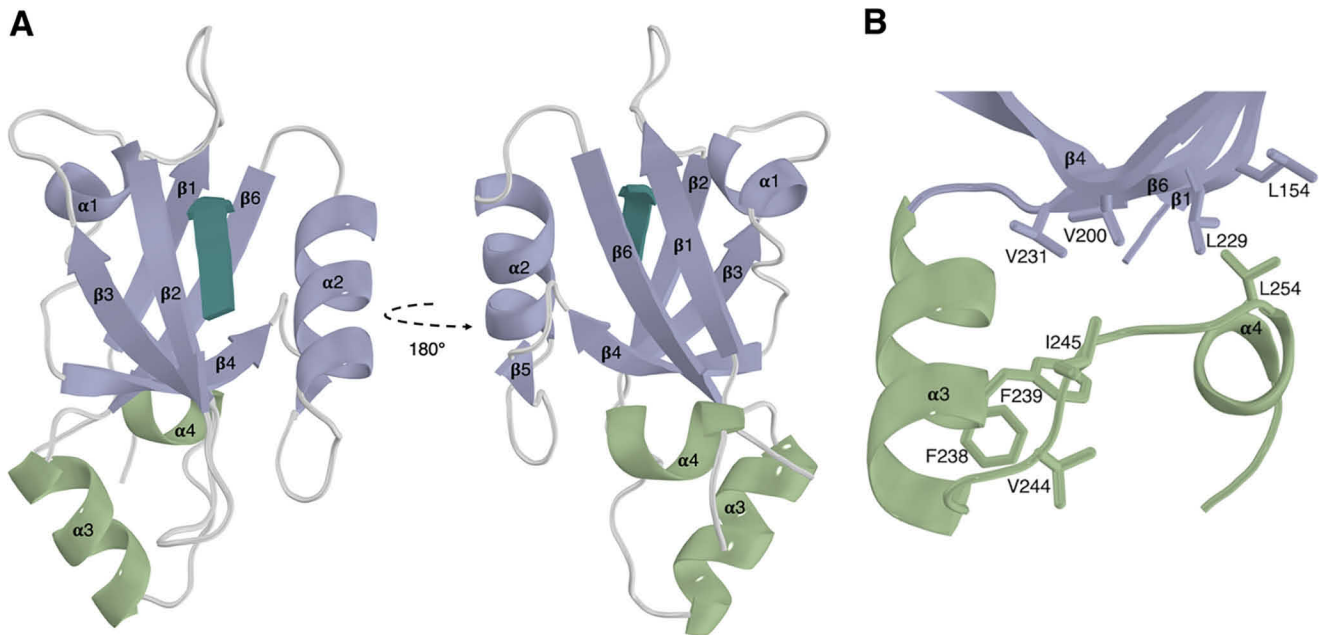
**Figure 1. The extended PDZ2 domain of NHERF1 in complex with the CFTR PDZ-binding motif.** *A,* the extended helical regions (*green*) couple to the canonical PDZ domain (*purple*) at a region distal to the PDZ-binding motif (*teal*). *B,* hydrophobic interactions formed between the α3 and α4 and β1, β4, and β6 from the core PDZ-fold.
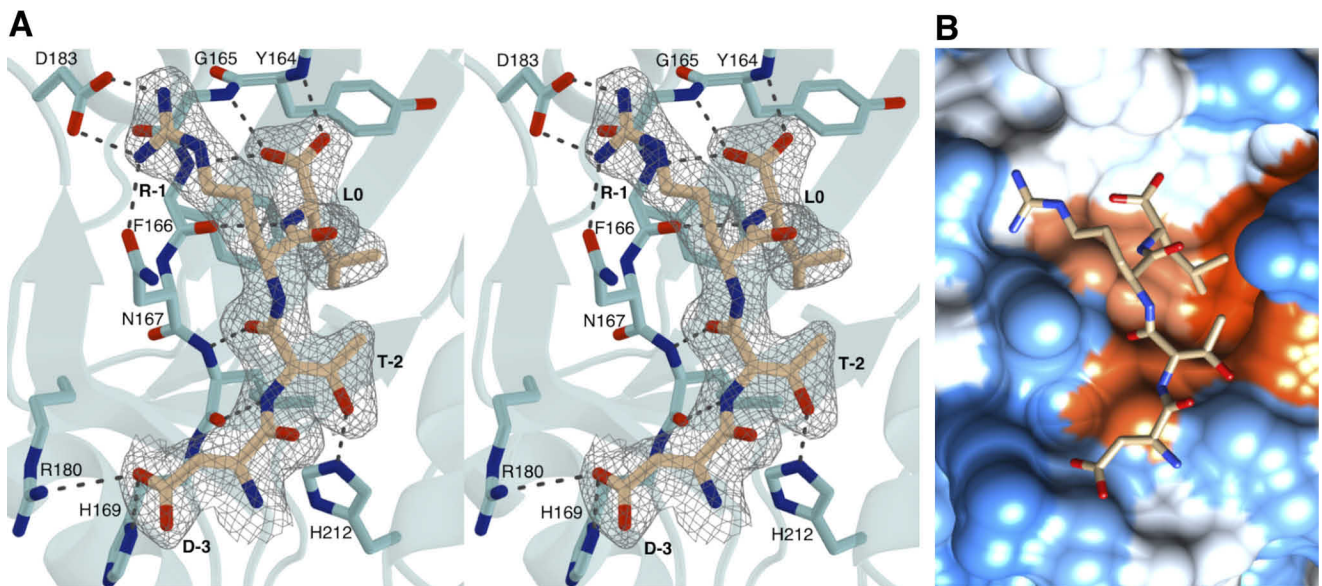


**Figure 2. Interactions between NHERF1 PDZ2 and CFTR.** *A,* stereo view of the NHERF1 PDZ2-binding site (*cyan*) bound to the PDZ-binding motif of CFTR (*beige*). The $2F_o - F_c$ map is shown around the CFTR PDZ-binding motif contoured at 1.0 σ within 1.5 Å of the selected atoms. *B,* hydrophobicity surface structure of the NHERF1 PDZ2-binding site based on the Kyte-Doolittle scale with the most hydrophillic regions shown in *blue* and most hydrophobic regions shown in *orange-red*. The CFTR PDZ-binding motif is shown as a stick model in *beige*. Image was generated using Chimera (60).

PDZ-binding motif. A number of constructs were generated in which residues of the CFTR PDZ-binding motif were mutated to alanine, as well as a phosphomimetic motif in which the threonine of the PDZ-binding motif was mutated to glutamic acid (Fig. 5*A*). On co-transfection with GFP-PDZ constructs, visual comparison indicated that these substitution mutants demonstrated lower levels of crystal fluorescence than the iBox-PAKcat-DTRL construct (Fig. 5*B*, Fig. S7). In particular, introduction of the C-terminal leucine to alanine substitution mutant (iBox-PAK4cat-DTRA) had a drastic effect, with crystal fluorescence levels appearing sim-

ilar to the iBox-PAK4cat-AAAA negative control (Fig. 5*B*, Fig. S7). That such a large effect comes from a relatively conservative amino acid change may be understood by the stereochemical adaptation of the binding pocket to leucine observed in the crystal structure (Fig. 2*B*).

To characterize these constructs further, we sought to quantify the intensity of GFP fluorescence within the crystals. To remove background fluorescence caused by GFP-PDZ expression in the surrounding cells, crystal-containing cells were lysed, and crystals were imaged in a cell-free form (Fig. S9). For co-transfections employing iBox-PAK4cat-DTRA constructs,
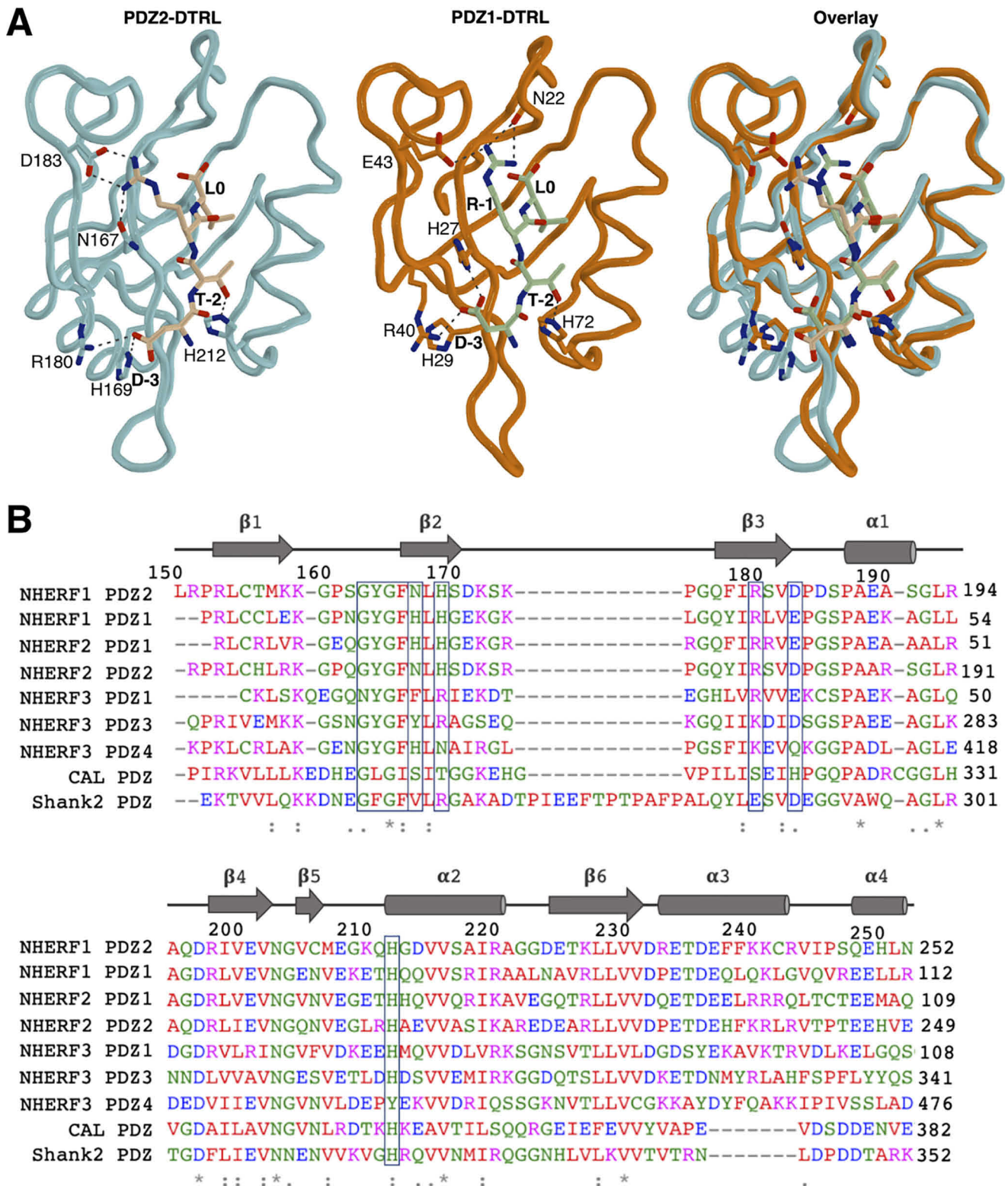
**Figure 3. Comparison of human CFTR-binding PDZ domains.** *A,* NHERF1 PDZ2-DTRL, NHERF1 PDZ1-DTRL (PDB 1I92), and overlay structures are shown as indicated. NHERF1 PDZ2-DTRL is shown as previously. NHERF1 PDZ1 is shown in *orange* and the PDZ-binding motif of CFTR in *green*. In both cases side chain groups of residues relevant to the ligand interaction are indicated. *Black dashes* represent bond distances measuring 3.3 Å or less. *B,* multiple sequence alignment of known CFTR-binding PDZ domains. Residue numbers and secondary structure of NHERF1 PDZ2 are indicated *above*. Conserved "*X-φ-G-φ*" carboxylate-binding loop and key residues within the PDZ-binding pocket, including D183/E43, are *boxed*.

levels of fluorescence were not above control levels. For the remaining constructs, quantitative analysis indicated that ATRL, DARL, DTAL, and DERL containing iBox-PAK4cat constructs demonstrated significantly lower levels of fluorescence than that of iBox-PAK4cat-DTRL (Fig. 5C). As such, it is evident that all residues of the CFTR "DTRL" PDZ-binding
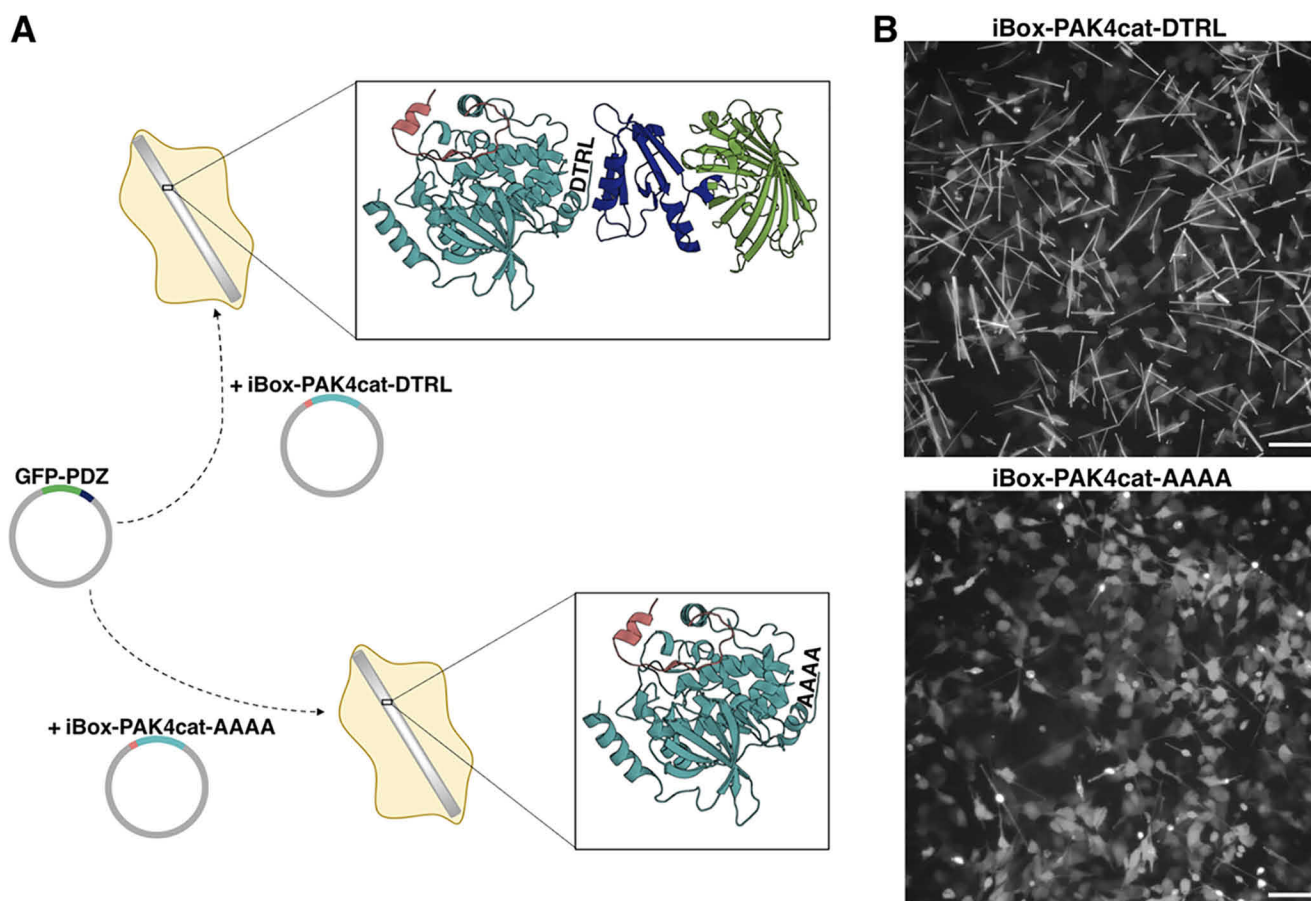
**A**



**B**

iBox-PAK4cat-DTRL



iBox-PAK4cat-AAAA

**Figure 4. Use of iBox-PAK4cat *in cellulo* crystals as a tool for studying protein-protein interactions.** *A,* schematic of the iBox-PAK4cat PPI assay. Mammalian cells are co-transfected with GFP-PDZ and iBox-PAK4cat constructs containing a C-terminal tetrapeptide motif (iBox-PAK4cat-DTRL and iBox-PAK4cat-AAAA). For iBox-PAK4cat-AAAA no interaction takes place and GFP-PDZ is not incorporated into the iBox-PAK4cat crystal lattice. Conversely, for iBox-PAK4cat-DTRL a PDZ domain-motif interaction occurs and GFP-PDZ is incorporated into the iBox-PAK4cat crystal lattice. The iBox-PAK4cat (*red* and *teal,* respectively) *in cellulo* crystal structure (PDB 4XBR) bound to GFP-PDZ (*green* and *blue,* respectively) is modeled for illustrative purposes only. *B,* fluorescent images of cells co-transfected with GFP-NHERF1 PDZ1 and iBox-PAK4cat-DTRL or iBox-PAK4cat-AAAA, as indicated. Equivalent transmitted light images are shown in Fig. S6. *Scale bar bottom right* indicates 100 $\mu$m.

motif form specific interactions within the binding pockets of NHERF1 PDZ1 and PDZ2.

### Molecular dynamics simulations and binding free energy studies on NHERF1 PDZ2-CFTR complex

The crystal structure presented here, supported by the findings of the novel iBox-PAK4cat *in cellulo* PPI assay, indicate that side chain-mediated interactions within the NHERF1 PDZ2-binding pocket enable the specific recognition of the CFTR PDZ-binding motif. To explore these findings further, *in silico*, molecular dynamics (MD) simulations were performed.

Following evaluation and verification of the protonation states of the histidine residues within the binding pocket ("Experimental procedures," Fig. S10), MD simulations were carried out using the obtained NHERF1 PDZ2-DTRL crystal structure. Simulations confirmed the persistence of hydrogen bonds observed in the crystal structure. R-1 was found to steadily form a salt bridge with the carboxylate of Asp[183], as the interactions between the carboxylic group of the D-3 with the guanidine group of Arg[180] and the side chain of His[169]. Similarly, the interaction between the hydroxyl group of T-2 and the side chain of His[212] showed a clear occupancy for 83–85% of the 50-ns production run. Two different binding modes could

be observed for the terminal carboxylate group of L0: the first, similar to the initial structure and involving direct interaction with the conserved GYGF carboxylate-binding motif; the second, with the terminal carboxylate shifted and more inclined toward Arg[220] in the opposite direction (Fig. 6). Surprisingly, in this mode, the initial direct interactions between the L0 terminal carboxylate and the GYGF motif are mediated by a water molecule that steadily occupies the space vacated by the carboxylate during its shift toward Arg[220]. This water molecule forms a network of interactions involving L0 and the GYGF motif when there are no direct interactions among the residues. A shift in the R-1 side chain could also be observed, enabling the interaction of the R-1 side chain with the backbone carbonyl of Ser[162] and a strong stabilization of the already present interaction with the amidic carbonyl group of the Asn[167] side chain. This orientation of the R-1 side chain appears to be an intermediate between those observed in the PDZ1 and PDZ2 crystal structures (Fig. 3A), and is coupled with L0 carboxylate shift and tightening of the $\beta1-\beta2$ loop (Fig. 6).

To confirm the findings of the iBox-PAK4cat protein-protein interaction assay, the same protocol was utilized to perform MD simulations on NHERF1 PDZ2 in complex with the
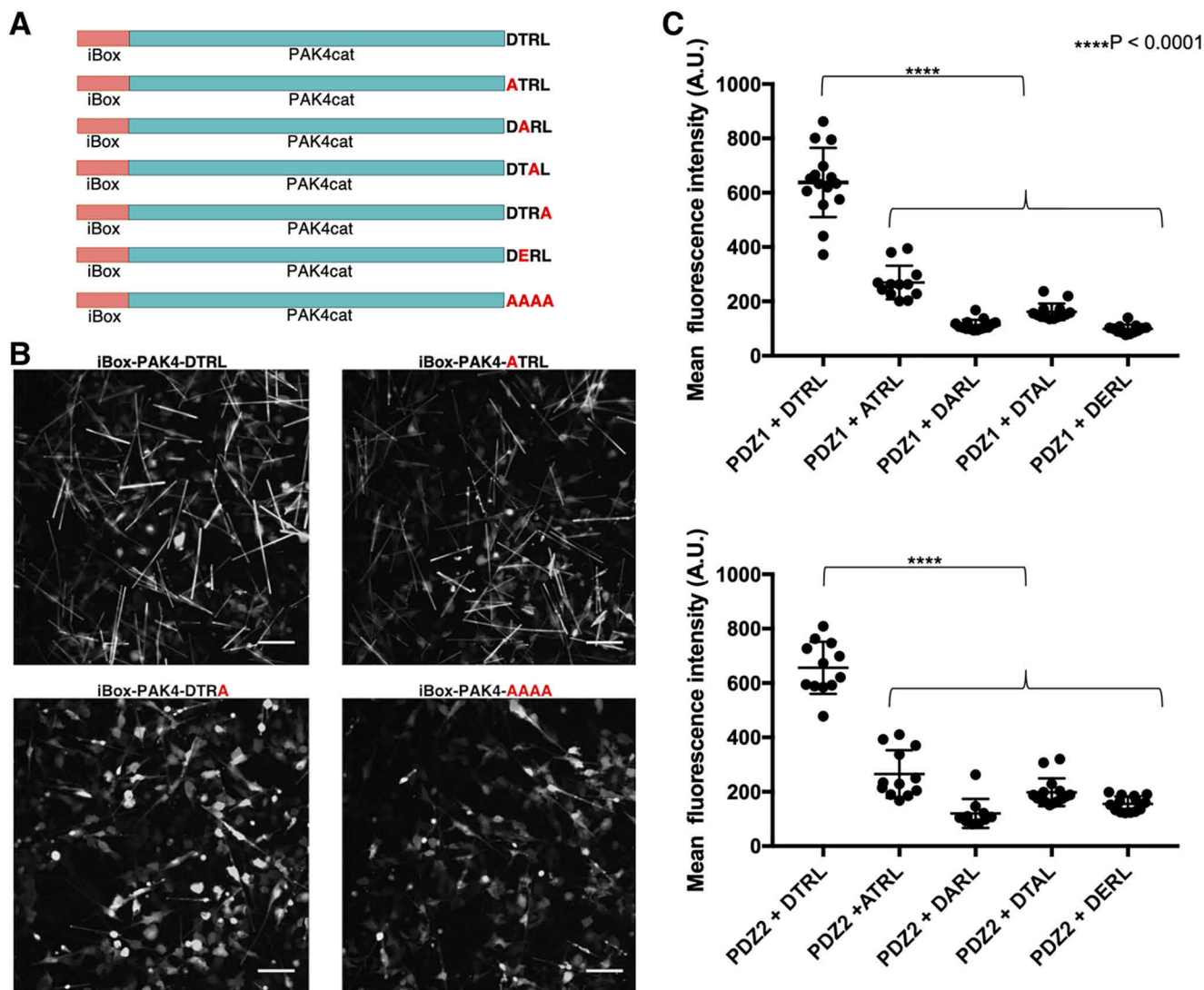
**Figure 5. Effect of PDZ-binding motif mutations on GFP integration into iBox-PAK4cat crystals.** *A,* iBox-PAK4cat constructs utilized in this study. *B,* fluorescent images of cells co-transfected with GFP-NHERF1 PDZ2 and iBox-PAK4cat constructs, as indicated. A full array of images obtained for the co-transfections can be seen in Fig. S7 and equivalent transmitted light images are shown in Fig. S8. *Scale bar bottom right* indicates 100 $\mu$m. *C,* substitution mutations of the DTRL PDZ-binding motif are associated with significantly lower levels of fluorescence within iBox-PAK4cat crystals (two-way ANOVA with Sidak's multiple comparisons test, $F_{(4, 122)} = 287$, $p < 0.0001$). Each point represents the mean fluorescence intensity of a single image containing multiple crystals, as shown in Fig. S9. $n = 10-15$.

ATRL, DARL, DTAL, and DTRA alanine substitution mutants of the PDZ-binding motif. For these simulations, the RMSD values related to the secondary structure elements were found to remain in the same range as for the WT complex. However, the stability of the peptide for all alanine substitution mutants was found to be much lower (Fig. S11), presumably due to the absence of key interactions within the binding pocket. To determine the effect of these mutations on interaction affinity, binding free energies for both replicates were calculated using both the solvation interaction energies (SIE) and molecular mechanics Poisson-Boltzmann surface area (MM-PBSA) methods (Table 2). During the initial evaluation of different protonation states on the WT simulations, the estimated binding energies were all found to be in agreement using both methods. However, with the MM-PBSA method only the ATRL and the DTAL systems were found to be substantially less favorable in terms of binding energies, whereas using the SIE method,

and in agreement with the findings of the iBox-PAK4cat PPI assay, all alanine substitution mutants were found to be less energetically favorable than the WT motif. In particular, the presence of the guanidino group at P-1 appears to be critical to the formation of interactions within the binding pocket, with a decrease over 4 kcal/mol (SIE method) and 15 kcal/mol (MM-PBSA) observable for both replicas of the DTAL system.

## Discussion

The findings presented here corroborate published data, which indicate that NHERF1 PDZ2 contains structured extensions outside of the core PDZ-fold (16, 17). Structured extensions outside of the canonical PDZ domain are not unique to NHERF1 PDZ2. NHERF1 PDZ1 has been shown to contain a highly similar C-terminal helical region, albeit with only comparatively negligible effects on stability and ligand binding affinity (17). The results presented here indicate that similar
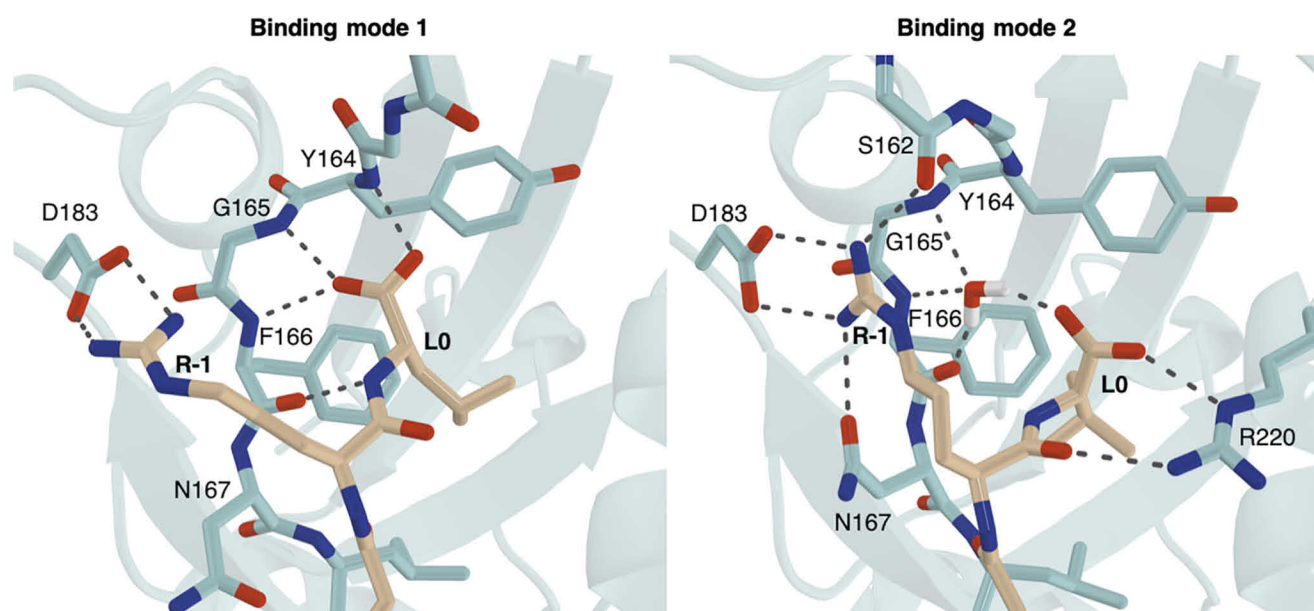
**Figure 6. Binding modes observed for L0 and R-1 in molecular dynamics simulations.** The two binding modes shown correspond to a 50:50 distribution between the two states. Representative frames of two binding modes were selected after clustering of two MD simulations. NHERF1 PDZ2 is colored in *cyan* and the CFTR PDZ-binding motif in *beige*. *Black dashes* represent bond distances measuring 3.3 Å or less. For clarity, hydrogens are shown for the water molecule only.

**Table 2**

**Binding free energies for WT and alanine mutants with MMPBSA and SIE methods**

|  | ΔG kcal/mol | ΔG kcal/mol | ΔG kcal/mol | ΔG kcal/mol | ΔG kcal/mol |
|---|---|---|---|---|---|
|  | (± S.E.) DTRL | (± S.E.) ATRL | (± S.E.) DARL | (± S.E.) DTAL | (± S.E.) DTRA |
| MM-PBSA | −73.24 ± 0.37 | −63.17 ± 0.34 | −72.66 ± 0.35 | −51.37 ± 0.52 | −72.46 ± 0.40 |
|  | −75.51 ± 0.40 | −64.55 ± 0.30 | −74.72 ± 0.38 | −58.28 ± 0.33 | −73.69 ± 0.34 |
| SIE | −14.53 ± 0.05 | −10.88 ± 0.03 | −11.33 ± 0.03 | −10.46 ± 0.04 | −11.27 ± 0.03 |
|  | −15.08 ± 0.03 | −10.93 ± 0.02 | −11.51 ± 0.03 | −10.36 ± 0.02 | −11.43 ± 0.03 |

structured extensions are common to several members of the NHERF family (Fig. 3*B*, Fig. S2). Indeed, bioinformatics studies have suggested that 40% of PDZ domains contain structured extensions outside of the core PDZ-fold (34). One of the best characterized examples to date is the third PDZ domain of PSD-95, which also contains a C-terminal α3 helix. The overall characteristics of this C-terminal extension are very similar to the extended region of NHERF1 PDZ2 in that (i) the extension is distal to the binding site, (ii) the extension does not induce any major structural changes, and (iii) the extension increases binding affinity for the ligand 21-fold (35). As such, extension mediated allosteric stabilization of the binding site may be a common mechanism shared among several PDZ domains. Further structural and biochemical studies are required to further elucidate the role of these structured extensions across the NHERF family.

This study has also provided further insight into the determinants of interaction between NHERF1 PDZ2 and the CFTR PDZ-binding motif. Although previous studies had suggested that the Glu[43] to Asp[183] substitution in PDZ2 was the sole determinant for the reduced binding affinity of NHERF1 PDZ2 to the CFTR C terminus relative to PDZ1 (17, 33), the crystal structure presented here demonstrates that Asp[183] is able to maintain the interaction with R-1 (Fig. 2*A*). These findings were confirmed by MD simulations, where this salt bridge interaction is found to be steady for the entire production (Fig. 6), indicating that the higher binding affinity achieved by NHERF1

PDZ1 is likely to be a result of a variety of structural features throughout the binding pocket, rather than sequence variation of a single residue. Interestingly, the MD simulations indicated two distinct binding modes for R-1 and L0 within the binding pocket. In addition to the canonical interaction between L0 and the carboxylate-binding loop, L0 can also be observed to shift toward Arg[220], with a water molecule instead facilitating the indirect interaction between the carboxylate group and the GYGF motif. Water-mediated hydrogen bonds between the terminal residue of the binding motif and the PDZ-binding pocket have been reported previously (28, 36), although the mode observed here appears to be mechanistically distinct. This orientation of L0 is also associated with the formation of a hydrogen bond between the R-1 side chain with the backbone carbonyl of Ser[162], a finding that is consistent with previous reports that phosphorylation of Ser[162] disrupts the interaction between NHERF1 PDZ2 and the PDZ-binding motif of CFTR (15).

The novel iBox-PAK4cat protein-protein interaction assay presented here has provided further insight into the determinants of the interaction between NHERF1 and CFTR. This approach allows clear differentiation between PDZ domain-binding (iBox-PAK4cat-DTRL) and nonbinding (iBox-PAK4cat-AAAA) motifs through visual comparison of crystal fluorescence (Fig. 4*B*). Introduction of the C-terminal leucine to alanine substitution mutant (iBox-PAK4cat-DTRA) had a drastic effect on GFP integration into the crystals, with crystal

fluorescence levels appearing similar to the iBox-PAK4cat-AAAA negative control (Fig. 5*B*). Such a finding is supported by co-immunoprecipitation data (37) and is consistent with the finding that the binding pocket is stereochemically adapted for the accommodation of the leucine side chain (Fig. 2*B*). As such, it is likely that the much smaller side chain of alanine would produce a much less energetically favorable interaction. The phosphomimetic motif-containing iBox-PAK4cat-DERL construct was also found to result in reduced fluorescence levels (Fig. 5*C*). Phosphorylation of the serine or threonine residues at this position has been demonstrated to disrupt the PDZ domain-motif interaction in several other cases (38–40). Although phosphorylation of this residue in CFTR has been hypothesized previously (15), the role of phosphorylation as a regulatory mechanism for this interaction requires further investigation.

Quantitative analysis of iBox-PAK4Cat-ATRL, iBox-PAK4Cat-DARL, and iBox-PAK4cat-DTAL constructs indicated that these PDZ-binding motif mutants had significantly lower levels of GFP integration into iBox-PAK4cat crystals than the WT CFTR PDZ-binding motif (Fig. 5*C*). This supports the finding, as demonstrated by the crystal structure (Fig. 2*A*), that interactions within the binding pocket enable the specific recognition of the aspartate, threonine, and arginine residues of the CFTR PDZ-binding motif. These findings were corroborated by MD and binding free energy studies, where the alanine substitution mutants were found to be less energetically favorable than the WT-binding motif. Interestingly, ATRL and DTAL sequences correspond to the PDZ-binding motifs of the sodium-dependent phosphate co-transporter and the $H^+$-ATPase, respectively, both of which have been shown to bind to the PDZ domains of NHERF1 (33, 41–43). As such, the PDZ-binding motif of CFTR appears to be an optimal PDZ-binding motif for interaction with the PDZ domains of NHERF1. This indicates that whereas the consensus motif $X$-S/T-$X$-$\Phi$ represents the minimal requirements for interaction with type I PDZ domains, residue selection at P-1 and P-3 does appear to influence the affinity of the interaction. There are several instances where competition between different PDZ domain-containing proteins has been shown to play a role in dynamic regulation of cell signaling (10, 13, 44, 46). As such, the ability of PDZ domains to bind to both optimal and suboptimal motifs may be key to maintaining promiscuity of the PDZ domain-motif interaction, whereas also allowing certain interactions to take precedence over others in the context of the PDZ domain interaction network.

Although the assay in its current state is best described as semi-quantitative, the results presented here provide proof-of-principle that iBox-PAK4cat crystals represent a potentially useful tool for the study of PDZ domain-motif interactions in a cellular context. The advantages of the iBox-PAK4cat system for detecting PDZ-motifs are clear: the assay is *in cellulo*, robust, quick, with the simple readout of fluorescence, and thus is a simple assay to introduce into a cell biology laboratory. We have demonstrated here that two PDZ domains can be easily screened against a number of interacting motifs. This strategy could easily be adapted to a high-throughput format allowing for multiple PDZ domains to be screened against multiple

interaction motifs. Indeed, this assay could be adapted to probe other protein-protein interactions, provided that both interaction partners can be accommodated within the iBox-PAK4cat crystal lattice.

## Experimental procedures

### Cloning and constructs

For the generation of NHERF1 PDZ2-DTRL, cDNA for human NHERF1 PDZ2 (NHERF1 residues 150–270) was cloned into pSY5 vector (47) using standard ligation-independent cloning methods (48). The CFTR PDZ-binding motif (CFTR residues 1477–1480) was inserted downstream using a QuikChange II Site-directed Mutagenesis Kit (Agilent) according to the manufacturer's instructions. For the generation of iBox-PAK4cat-DTRL, iBox-PAK4cat-ATRL, iBox-PAK4cat-DARL, iBox-PAK4cat-DTAL, iBox-PAK4cat-DTRA, iBox-PAK4cat-DERL, and iBox-PAK4cat-AAAA constructs, the relevant tetrapeptide motifs were inserted into iBox-PAK4cat within the pXJ40 vector (1) using the QuikChange II Site-directed Mutagenesis Kit (Agilent) according to the manufacturer's instructions. For the generation of GFP-PDZ1 and GFP-PDZ2 constructs, NHERF1 PDZ1 (NHERF1 residues 11–120) and PDZ2 (NHERF1 residues 150–270) domains were inserted into the multiple cloning site of pXJ40-GFP (49) using XhoI and KpnI restriction sites according to standard PCR restriction cloning methods. In all cases the presence of the desired construct was confirmed through sequencing.

### Expression, purification, and crystallization of PDZ2-DTRL

NHERF1 PDZ2-DTRL was expressed in *Escherichia coli* BL21 (DE3) (New England BioLabs). Cultures in autoinduction media (12 g/liter of tryptone, 24 g/liter of yeast extract, 9.4 g/liter of $K_2HPO_4$, 2.2 g/liter of $KH_2PO_4$, 8 ml/liter of glycerol, 50 mM $NH_4Cl$, 20 mM $MgSO_4$, 5 mM $Na_2SO_4$, 0.3% (w/v) $\alpha$-lactose, 0.015% (w/v) D-glucose) were grown at 37 °C until an $OD_{600}$ of 0.6–0.8, following which they were grown overnight at 15 °C. Cultures were harvested by centrifugation and pelleted cells were resuspended in 50 mM Tris·HCl, pH 8.0, 500 mM NaCl, and 20 mM imidazole. Cells were lysed using sonication and the cell lysate was clarified through centrifugation. All purification steps were carried out using the ÅKTA Express Purification System (GE Healthcare). Lysates were loaded onto a 5-ml HisTrap FF nickel-nitrilotriacetic acid column (GE Healthcare). The column was washed with 50 mM Tris·HCl, pH 8.0, 500 mM NaCl, and 20 mM imidazole prior to elution of bound proteins with 50 mM Tris·HCl, pH 8.0, 500 mM NaCl, and 250 mM imidazole. The eluted material was collected and exchanged into 50 mM Tris·HCl, pH 8.0, on a HiPrep 26/10 desalting column (GE Healthcare). Eluted proteins were loaded onto a 1-ml HiTrap Q HP column (GE healthcare) for anion-exchange chromatography. Bound proteins were eluted using a gradient of 0–500 mM NaCl, followed by a final elution with 1 M NaCl. Eluted fractions were analyzed using SDS-PAGE. Relevant fractions were combined and further purified by size-exclusion chromatography in 50 mM Tris·HCl, pH 8.0, 150 mM NaCl using a HiLoad 16/600 Superdex 75 column (GE Healthcare). The protein eluted as a single peak and eluted fractions were analyzed using SDS-PAGE and Coomassie Brilliant Blue

staining. Fractions of sufficient purity were combined and concentrated in a 10-kDa molecular mass cut-off concentrator. Protein concentration was determined using the Pierce bicinchoninic acid protein assay kit (Thermo Scientific) according to the manufacturer's instructions. Crystallization was carried by mixing 2 $\mu$l of 10.5 mg/ml of protein solution with 1 $\mu$l of 1.65 M ammonium sulfate and 100 mM trisodium citrate, pH 5.6, using the hanging drop diffusion method. Bipyramidal-shaped crystals grew at 15 °C, taking approximately one month to grow to full size at which point they measured 50 $\mu$m at their widest dimension.

### X-ray data collection and structure determination

Crystals were harvested into mother liquor containing 30% (v/v) glycerol and flash-frozen in liquid nitrogen. X-ray diffraction data for NHERF1 PDZ2-DTRL were collected remotely at the Australian Synchrotron. Data were collected using an ADSC Quantum 315r CCD detector at the MX2 beamline at a wavelength of 1.0 Å. Each image covered an oscillation of 0.5 degrees. Images were indexed and integrated using MOSFLM (50). The space group was determined to be $I2_12_12_1$ using POINTLESS and the data were scaled using AIMLESS, both within the CCP4 suite of programs (51). The structure was solved by molecular replacement in PHASER (52) using the structure of NHERF1 PDZ2 bound to the CXCR2 PDZ-binding motif (PDB 4Q3H) as a search model. The solvent content was determined to be 50.1% with a Matthews coefficient ($V_m$) of 2.50 Å$^3$/Da. This is consistent with the presence of two complexes within the asymmetric unit. Manual building of the extended PDZ domain and PDZ-binding motif was carried out in Coot molecular graphics software (53). The structure was refined to a resolution of 2.20 Å using phenix.refine (54), yielding a final $R_{work}/R_{free}$ of 0.2360/0.2752. In the final round of refinement a twinning correction was applied (-h,-k,-l), which resulted in a 4% drop in the $R_{free}$ value. All figures depicting the structure were generated in PyMOL (55), unless otherwise stated.

### Transfection of cell culture

Monkey COS-7 cells were grown in high-glucose Dulbecco's modified Eagle's medium (HyClone) supplemented with 10% (v/v) bovine calf serum (HyClone). Cells were incubated at 37 °C with 5% $CO_2$. Transfections were carried out using jetPEI transfection reagent (Polyplus transfection) according to the manufacturer's instructions.

### Live cell imaging of crystal growth

Relevant constructs were co-transfected into COS-7 cells in 24-well black-walled glass-bottomed $\mu$-plate (Ibidi). Immediately after transfection, images were acquired on an Eclipse Ti inverted microscope (Nikon) using a 10 × 0.3 SPlan Fluar objective, the filter sets for GFP, and a pE-300 LED (CoolLED) fluorescent light source. Imaging software NIS Elements AR.46.00.0.point visiting was used to allow five positions to be imaged for each well within the same time course. Images were collected using a CoolSnap Monochrome camera (Photometrics) every 30 min for a total of 71.5 h. GFP fluorescence images were acquired using a fixed exposure time of 200 ms. Transmit-ted light images were acquired using a fixed exposure time of 50 ms. Cells were maintained at 37 °C and 5% $CO_2$ throughout the course of the experiment.

### Cell breakage and separation of iBox-PAK4cat crystals

Relevant constructs were co-transfected into COS-7 cells in 6-well dishes. Three days post-transfection, Dulbecco's modified Eagle's medium was aspirated from the cells and 500 $\mu$l of hypotonic lysis buffer (50 mM Tris·HCl, pH 7.4, 25 units/ml of DNase I (Promega), 0.2% (v/v) Triton X-100) was added to each well. Plates were rocked at ambient temperature until cells could be observed to detach from the plate. Lysed cells were centrifuged in a square-bottomed cuvette at ambient temperature for 5 min at 200 × $g$ in a bench-top centrifuge, such that the pellet contained cell debris and the supernatant contained crystals. Supernatants were aspirated into a black-walled glass-bottomed 24-well plate (Ibidi) for imaging.

### Crystal imaging and quantification of GFP fluorescence

Harvested crystals were imaged in 24-well black-walled glass-bottomed $\mu$-plate (Ibidi) on an MMI CellCut laser microdissection system (Olympus) using a 10 × 0.3 UPlan FLN objective, the filter sets for FITC, and a xenon mercury fluorescent light source. Images were collected using an Orca ER C4742-95-12ERG monochrome camera (Hamamatsu) using a fixed exposure time of 100 ms. Fluorescence intensity quantification was carried out using Fiji software (56). Crystal-containing regions were selected using automatic thresholding with the Otsu algorithm and the mean gray value was measured. The acquired values were plotted and subjected to two-way ANOVA with Sidak's multiple comparisons test using GraphPad Prism 7.0 software.

### Multiple sequence alignments

Multiple sequence alignment was carried out with ClustalW2 using the default settings (57).

### Models building and molecular dynamics simulations

The initial NHERF1 PDZ2-DTRL complex was edited to consider only the sequence portion interacting with the NHERF1 PDZ2 core domain. Subsequently the DTRL portion of the WT peptide was modified to obtain the corresponding alanine mutants (ATRL, DARL, DTAL, and DTRA). The systems were modeled using the Protein Preparation Wizard tool (58) of the Schrödinger Suite and the protonation states of His[169] and His[212] were evaluated and verified using the PropKa routine at pH 7.0 ± 0.2 as default. Although on initial evaluation both histidines were estimated to be in HID form (neutral, $\delta$-nitrogen protonated), on further analysis with the PropKa routine, His[212] was estimated to be in the HIE state (neutral, $\epsilon$-nitrogen protonated) with a p$K_a$ of 5.20, whereas His[169] was evaluated to be present in the HIP state (+1 charged, both $\delta$- and $\epsilon$-nitrogens protonated) with a p$K_a$ value of 7.13. As a consequence, four combinations of protonation states for His[169] (HID/HIP) and His[212] (HID/HIE) of NHERF1 PDZ2 were evaluated. For each combination, two replicate 50-ns production runs were performed and evaluated to assess the persistence of the p$K_a$ values obtained during initial settings. Frames at

defined time steps (every 5–10 ns) were selected and evaluated. All the investigated frames of WT simulations reporting HIP169 demonstrated a well-maintained HIP state as predicted in earlier phases. The RMSD of the C$\alpha$ atoms was evaluated for: 1) the whole complex, 2) the secondary structure of the PDZ2 domain, and 3) the CFTR PDZ-binding motif (Fig. S10). Generally, the RMSD value of the C$\alpha$ atoms in the secondary structure was found to remain below 1.0 Å in all of the systems. Nevertheless, an improved stabilization of the peptide was observed for simulations reporting the HIP state for His[169]. In particular, for the HIP169/HID212 state, the RMSD value related to the C$\alpha$ atoms was found to oscillate between 1.0 and 3.0 Å and the calculated binding free energies with both MM-PBSA and the SIE methods indicated that this system had much higher stability than the other systems. As such, our analyses focused on the HIP169/HID212 replicas. For simulations employing the DARL, DTAL, and DTRA alanine substitution mutants, the same protonation states as described for the WT complex were employed. However, for the ATRL alanine substitution mutant, the absence of aspartate at the P-3 of the binding motif was found to significantly change the local environment so that the p$K_a$ value of His[169] was decreased. As a result, for this system only the $\epsilon$ nitrogen of His[169] was considered to be protonated. This procedure has been repeated to verify the p$K_a$ at fixed time steps during all simulations. MD simulations were carried out using the AMBER package, version 14 (59). All complexes were placed in a rectangular parallel piped waterbox and solvated with a 25 Å water cap, employing the TIP3P explicit solvent model and different counterions to neutralize the systems. Simulations were conducted using the ff14SB force field at 300 K, the particle mesh Ewald method for long-range electrostatic interactions, and periodic boundary conditions. A cut-off of 10 Å for the nonbonded interactions was also included and the general time step for all simulations was set as 2.0 fs. The SHAKE algorithm was applied to keep all bonds involving hydrogen atoms rigid. Prior to the simulations, each system was subjected to an energy minimization using the steepest descent algorithm, followed by conjugate gradient. The temperatures of the systems were raised from 0 to 300 K within 500 ps of simulation time under constant-volume periodic boundary condition. During both stages, all C$\alpha$ atoms of the complexes were kept restrained with a harmonic force constant of 10 kcal/mol·Å$^2$. Multiple equilibration stages were lately performed with a constant-pressure periodic boundary condition and a gradual decrease of the harmonic force constant, until the whole system was completely relaxed. During this stage (equivalent to 3–5 ns), the pressure and the temperature of the systems were kept constant by employing the Monte Carlo barostat (with anisotropic pressure scaling) and the Langevin thermostat. Molecular dynamics productions were finally carried out with the same temperature and pressure conditions but without restraints for a singular amount of 50 ns for each peptide-protein complex. The CPPTRAJ and PTRAJ modules of AmberTools were employed to process and analyze all trajectories, whereas UCSF Chimera (60) was utilized for visualization and preliminary inspections. RMSD plots and all images were generated using, respectively, Gnuplot and PyMOL (55).

### Binding free energy studies

Binding energy studies were carried out by applying the MM-PBSA (61–63) method as general standard and SIE method (11–14) in line with an approach employed previously (15). For the calculation of binding energies using the MM-PBSA method (61–63), the MM-PBSA implementation of the AMBER 14 package was used (59). The Van der Waals, electrostatics, and internal interaction were estimated by employing the SANDER module, whereas the MM-PBSA module was used to calculate polar energies. Dielectric constants of 1 and 80 were applied to represent the gas and water phases, respectively. MOLSURF was employed to estimate the nonpolar energies, whereas the entropic term was deemed as approximately constant compared with the systems interactions. For the calculation of binding energies using the SIE method, an adapted version of the SIETRAJ tool (available at RRID:SCR_018021) was used. The SIETRAJ tool employed several scripts based on a Tcl runtime library (BRIMM) and its internal Poisson solver and surface generation methods (45, 64, 65).

### Accession codes

Atomic coordinates and structure factor files have been deposited in the Protein Data Bank under accession code 6RQR.

### References

1. Baskaran, Y., Ang, K. C., Anekal, P. V., Chan, W. L., Grimes, J. M., Manser, E., and Robinson, R. C. (2015) An *in cellulo*-derived structure of PAK4 in complex with its inhibitor Inka1. *Nat. Commun.* **6,** 8681 CrossRef Medline
2. Letunic, I., and Bork, P. (2018) 20 years of the SMART protein domain annotation resource. *Nucleic Acids Res.* **46,** D493–D496 Medline
3. Songyang, Z., Fanning, A. S., Fu, C., Xu, J., Marfatia, S. M., Chishti, A. H., Crompton, A., Chan, A. C., Anderson, J. M., and Cantley, L. C. (1997) Recognition of unique carboxyl-terminal motifs by distinct PDZ domains. *Science* **275,** 73–77 CrossRef Medline
4. Schultz, J., Hoffmüller, U., Krause, G., Ashurst, J., Macias, M. J., Schmieder, P., Schneider-Mergener, J., and Oschkinat, H. (1998) Specific interactions between the syntrophin PDZ domain and voltage-gated sodium channels. *Nat. Struct. Biol.* **5,** 19–24 CrossRef Medline
5. Stricker, N. L., Christopherson, K. S., Yi, B. A., Schatz, P. J., Raab, R. W., Dawes, G., Bassett, D. E., Jr., Bredt, D. S., and Li, M. (1997) PDZ domain of neuronal nitric oxide synthase recognizes novel C-terminal peptide sequences. *Nat. Biotechnol.* **15,** 336–342 CrossRef Medline

6. Lukacs, G. L., and Verkman, A. S. (2012) CFTR: folding, misfolding and correcting the ΔF508 conformational defect. *Trends Mol. Med.* **18,** 81–91 CrossRef Medline

7. Southern, K. W., Munck, A., Pollitt, R., Travert, G., Zanolla, L., Dankert-Roelse, J., Castellani, C., and ECFS CF Neonatal Screening Working Group (2007) A survey of newborn screening for cystic fibrosis in Europe. *J. Cyst. Fibros.* **6,** 57–65 CrossRef

8. Riordan, J. R. (2008) CFTR function and prospects for therapy. *Annu. Rev. Biochem.* **2008,** 701–726 Medline

9. Farinha, C. M., and Amaral, M. D. (2005) Most F508del-CFTR is targeted to degradation at an early folding checkpoint and independently of calnexin. *Mol. Cell. Biol.* **25,** 5242–5252 CrossRef Medline

10. Cushing, P. R., Fellows, A., Villone, D., Boisguérin, P., and Madden, D. R. (2008) The relative binding affinities of PDZ partners for CFTR: a biochemical basis for efficient endocytic recycling. *Biochemistry* **47,** 10084–10098 CrossRef Medline

11. Hegedüs, T., Sessler, T., Scott, R., Thelin, W., Bakos, E., Váradi, A., Szabó, K., Homolya, L., Milgram, S. L., and Sarkadi, B. (2003) C-terminal phosphorylation of MRP2 modulates its interaction with PDZ proteins. *Biochem. Biophys. Res. Commun.* **302,** 454–461 CrossRef Medline

12. Kim, J. Y., Han, W., Namkung, W., Lee, J. H., Kim, K. H., Shin, H., Kim, E., and Lee, M. G. (2004) Inhibitory regulation of cystic fibrosis transmembrane conductance regulator anion-transporting activities by Shank2. *J. Biol. Chem.* **279,** 10389–10396 CrossRef

13. Lee, J. H., Richter, W., Namkung, W., Kim, K. H., Kim, E., Conti, M., and Lee, M. G. (2007) Dynamic regulation of cystic fibrosis transmembrane conductance regulator by competitive interactions of molecular adaptors. *J. Biol. Chem.* **282,** 10414–10422 CrossRef

14. Wang, S., Raab, R. W., Schatz, P. J., Guggino, W. B., and Li, M. (1998) Peptide binding consensus of the NHE-RF-PDZ1 domain matches the C-terminal sequence of cystic fibrosis transmembrane conductance regulator (CFTR). *FEBS Lett.* **427,** 103–108 CrossRef Medline

15. Raghuram, V., Hormuth, H., and Foskett, J. K. (2003) A kinase-regulated mechanism controls CFTR channel gating by disrupting bivalent PDZ domain interactions. *Proc. Natl. Acad. Sci. U.S.A.* **100,** 9620–9625 CrossRef Medline

16. Bhattacharya, S., Dai, Z., Li, J., Baxter, S., Callaway, D. J., Cowburn, D., and Bu, Z. (2010) A conformational switch in the scaffolding protein NHERF1 controls autoinhibition and complex formation. *J. Biol. Chem.* **285,** 9981–9994 CrossRef

17. Bhattacharya, S., Ju, J. H., Orlova, N., Khajeh, J. A., Cowburn, D., and Bu, Z. (2013) Ligand-induced dynamic changes in extended PDZ domains from NHERF1. *J. Mol. Biol.* **425,** 2509–2528 CrossRef Medline

18. Guerra, L., Fanelli, T., Favia, M., Riccardi, S. M., Busco, G., Cardone, R. A., Carrabino, S., Weinman, E. J., Reshkin, S. J., Conese, M., and Casavola, V. (2005) Na$^+$/H$^+$ exchanger regulatory factor isoform 1 overexpression modulates cystic fibrosis transmembrane conductance regulator (CFTR) expression and activity in human airway 16HBE14o-cells and rescues DeltaF508 CFTR functional expression in cystic fibrosis cells. *J. Biol. Chem.* **280,** 40925–40933 CrossRef

19. Loureiro, C. A., Matos, A. M., Dias-Alves, Á., Pereira, J. F., Uliyakina, I., Barros, P., Amaral, M. D., and Matos, P. (2015) A molecular switch in the scaffold NHERF1 enables misfolded CFTR to evade the peripheral quality control checkpoint. *Sci. Signal.* **8,** ra48 CrossRef Medline

20. Swiatecka-Urban, A., Duhaime, M., Coutermarsh, B., Karlson, K. H., Collawn, J., Milewski, M., Cutting, G. R., Guggino, W. B., Langford, G., and Stanton, B. A. (2002) PDZ domain interaction controls the endocytic recycling of the cystic fibrosis transmembrane conductance regulator. *J. Biol. Chem.* **277,** 40099–40105 CrossRef

21. Cheng, J., Moyer, B. D., Milewski, M., Loffing, J., Ikeda, M., Mickle, J. E., Cutting, G. R., Li, M., Stanton, B. A., and Guggino, W. B. (2002) A Golgi-associated PDZ domain protein modulates cystic fibrosis transmembrane regulator plasma membrane expression. *J. Biol. Chem.* **277,** 3520–3529 CrossRef

22. Sun, F., Hug, M. J., Bradbury, N. A., and Frizzell, R. A. (2000) Protein kinase A associates with cystic fibrosis transmembrane conductance regulator via an interaction with ezrin. *J. Biol. Chem.* **275,** 14360–14366 CrossRef

23. Monterisi, S., Favia, M., Guerra, L., Cardone, R. A., Marzulli, D., Reshkin, S. J., Casavola, V., and Zaccolo, M. (2012) CFTR regulation in human airway epithelial cells requires integrity of the actin cytoskeleton and compartmentalized cAMP and PKA activity. *J. Cell Sci.* **125,** 1106–1117 CrossRef Medline

24. Ostedgaard, L. S., Randak, C., Rokhlina, T., Karp, P., Vermeer, D., Ashbourne Excoffon, K. J., and Welsh, M. J. (2003) Effects of C-terminal deletions on cystic fibrosis transmembrane conductance regulator function in cystic fibrosis airway epithelia. *Proc. Natl. Acad. Sci. U.S.A.* **100,** 1937–1942 CrossRef Medline

25. Arora, K., Moon, C., Zhang, W., Yarlagadda, S., Penmatsa, H., Ren, A., Sinha, C., and Naren, A. P. (2014) Stabilizing rescued surface-localized DeltaF508 CFTR by potentiation of its interaction with Na$^+$/H$^+$ exchanger regulatory factor 1. *Biochemistry* **53,** 4169–4179 CrossRef Medline

26. Dev, K. K. (2004) Making protein interactions druggable: targeting PDZ domains. *Nat. Rev. Drug Discov.* **3,** 1047–1056 CrossRef Medline

27. Houslay, M. D. (2009) Disrupting specific PDZ domain-mediated interactions for therapeutic benefit. *Br. J. Pharmacol.* **158,** 483–485 CrossRef Medline

28. Karthikeyan, S., Leung, T., and Ladias, J. A. (2001) Structural basis of the Na$^+$/H$^+$ exchanger regulatory factor PDZ1 interaction with the carboxyl-terminal region of the cystic fibrosis transmembrane conductance regulator. *J. Biol. Chem.* **276,** 19683–19696 CrossRef

29. Karthikeyan, S., Leung, T., and Ladias, J. A. (2002) Structural determinants of the Na$^+$/H$^+$ exchanger regulatory factor interaction with the $\beta_2$ adrenergic and platelet-derived growth factor receptors. *J. Biol. Chem.* **277,** 18973–18978 CrossRef

30. Holcomb, J., Jiang, Y., Guan, X., Trescott, L., Lu, G., Hou, Y., Wang, S., Brunzelle, J., Sirinupong, N., Li, C., and Yang, Z. (2014) Crystal structure of the NHERF1 PDZ2 domain in complex with the chemokine receptor CXCR2 reveals probable modes of PDZ2 dimerization. *Biochem. Biophys. Res. Commun.* **448,** 169–174 CrossRef Medline

31. Elkins, J. M., Papagrigoriou, E., Berridge, G., Yang, X., Phillips, C., Gileadi, C., Savitsky, P., and Doyle, D. A. (2007) Structure of PICK1 and other PDZ domains obtained with the help of self-binding C-terminal extensions. *Protein Sci.* **16,** 683–694 CrossRef Medline

32. Li, J. Q., Poulikakos, P. I., Dai, Z. P., Testa, J. R., Callaway, D. J. E., and Bu, Z. M. (2007) Protein kinase c phosphorylation disrupts Na$^+$/H$^+$ exchanger regulatory factor 1 autoinhibition and promotes cystic fibrosis transmembrane conductance regulator macromolecular assembly. *J. Biol. Chem.* **282,** 27086–27099 CrossRef

33. Mamonova, T., Zhang, Q., Khajeh, J. A., Bu, Z., Bisello, A., and Friedman, P. A. (2015) Canonical and noncanonical sites determine NPT2A binding selectivity to NHERF1 PDZ1. *PLOS One* **10,** e0129554 CrossRef Medline

34. Wang, C. K., Pan, L. F., Chen, J., and Zhang, M. J. (2010) Extensions of PDZ domains as important structural and functional elements. *Protein Cell* **1,** 737–751 Medline

35. Petit, C. M., Zhang, J., Sapienza, P. J., Fuentes, E. J., and Lee, A. L. (2009) Hidden dynamic allostery in a PDZ domain. *Proc. Natl. Acad. Sci. U.S.A.* **106,** 18249–18254 CrossRef Medline

36. Doyle, D. A., Lee, A., Lewis, J., Kim, E., Sheng, M., and MacKinnon, R. (1996) Crystal structures of a complexed and peptide-free membrane protein-binding domain: molecular basis of peptide recognition by PDZ. *Cell* **85,** 1067–1076 CrossRef Medline

37. Moyer, B. D., Duhaime, M., Shaw, C., Denton, J., Reynolds, D., Karlson, K. H., Pfeiffer, J., Wang, S., Mickle, J. E., Milewski, M., Cutting, G. R., Guggino, W. B., Li, M., and Stanton, B. A. (2000) The PDZ-interacting domain of cystic fibrosis transmembrane conductance regulator is required for functional expression in the apical plasma membrane. *J. Biol. Chem.* **275,** 27069–27074 Medline

38. Cohen, N. A., Brenman, J. E., Snyder, S. H., and Bredt, D. S. (1996) Binding of the inward rectifier K$^+$ channel Kir 2.3 to PSD-95 is regulated by protein kinase A phosphorylation. *Neuron* **17,** 759–767 CrossRef Medline

39. Chetkovich, D. M., Chen, L., Stocker, T. J., Nicoll, R. A., and Bredt, D. S. (2002) Phosphorylation of the postsynaptic density-95 (PSD-95)/discs large/zona occludens-1 binding site of stargazin regulates binding to

PSD-95 and synaptic targeting of AMPA receptors. *J. Neurosci.* **22,** 5791–5796 CrossRef Medline

40. Choi, J., Ko, J., Park, E., Lee, J. R., Yoon, J., Lim, S., and Kim, E. (2002) Phosphorylation of stargazin by protein kinase A regulates its interaction with PSD-95. *J. Biol. Chem.* **277,** 12359–12363 CrossRef

41. Gisler, S. M., Stagljar, I., Traebert, M., Bacic, D., Biber, J., and Murer, H. (2001) Interaction of the type IIa Na/P$_i$ cotransporter with PDZ proteins. *J. Biol. Chem.* **276,** 9206–9213 CrossRef

42. Wang, B., Means, C. K., Yang, Y., Mamonova, T., Bisello, A., Altschuler, D. L., Scott, J. D., and Friedman, P. A. (2012) Ezrin-anchored protein kinase A coordinates phosphorylation-dependent disassembly of a NHERF1 ternary complex to regulate hormone-sensitive phosphate transport. *J. Biol. Chem.* **287,** 24148–24163 CrossRef

43. Breton, S., Wiederhold, T., Marshansky, V., Nsumu, N. N., Ramesh, V., and Brown, D. (2000) The B1 subunit of the H$^+$-ATPase is a PDZ domain-binding protein: colocalization with NHE-RF in renal B-intercalated cells. *J. Biol. Chem.* **275,** 18219–18224 CrossRef

44. Alewine, C., Olsen, O., Wade, J. B., and Welling, P. A. (2006) TIP-1 has PDZ scaffold antagonist activity. *Mol. Biol. Cell* **17,** 4200–4211 CrossRef

45. Cui, Q. Z., Sulea, T., Schrag, J. D., Munger, C., Hung, M. N., Naïm, M., Cygler, M., and Purisima, E. O. (2008) Molecular dynamics-solvated interaction energy studies of protein-protein interactions: the MP1-p14 scaffolding complex. *J. Mol. Biol.* **379,** 787–802 CrossRef Medline

46. Lee, S. J., Ritter, S. L., Zhang, H., Shim, H., Hall, R. A., and Yun, C. C. (2011) MAGI-3 competes with NHERF-2 to negatively regulate LPA2 receptor signaling in colon cancer cells. *Gastroenterology* **140,** 924–934 CrossRef Medline

47. Chumnarnsilpa, S., Lee, W. L., Nag, S., Kannan, B., Larsson, M., Burtnick, L. D., and Robinson, R. C. (2009) The crystal structure of the C-terminus of adseverin reveals the actin-binding interface. *Proc. Natl. Acad. Sci. U.S.A.* **106,** 13719–13724 CrossRef Medline

48. Aslanidis, C., and de Jong, P. J. (1990) Ligation-independent cloning of PCR products (LIC-PCR). *Nucleic Acids Res.* **18,** 6069–6074 CrossRef Medline

49. Manser, E., Huang, H. Y., Loo, T. H., Chen, X. Q., Dong, J. M., Leung, T., and Lim, L. (1997) Expression of constitutively active alpha-PAK reveals effects of the kinase on actin and focal complexes. *Mol. Cell. Biol.* **17,** 1129–1143 CrossRef Medline

50. Battye, T. G. G., Kontogiannis, L., Johnson, O., Powell, H. R., and Leslie, A. G. W. (2011) iMOSFLM: a new graphical interface for diffraction-image processing with MOSFLM. *Acta Crystallogr. D Biol. Crystallogr.* **67,** 271–281 CrossRef

51. Winn, M. D., Ballard, C. C., Cowtan, K. D., Dodson, E. J., Emsley, P., Evans, P. R., Keegan, R. M., Krissinel, E. B., Leslie, A. G. W., McCoy, A., McNicholas, S. J., Murshudov, G. N., Pannu, N. S., Potterton, E. A., Powell, H. R., Read, R. J., Vagin, A., and Wilson, K. S. (2011) Overview of the CCP4 suite and current developments. *Acta Crystallogr. Sect. D Biol. Crystallogr.* **67,** 235–242 CrossRef

52. McCoy, A. J., Grosse-Kunstleve, R. W., Adams, P. D., Winn, M. D., Storoni, L. C., and Read, R. J. (2007) Phaser crystallographic software. *J. Appl. Crystallogr.* **40,** 658–674 CrossRef Medline

53. Emsley, P., and Cowtan, K. (2004) Coot: model-building tools for molecular graphics. *Acta Crystallogr. D Biol. Crystallogr.* **60,** 2126–2132 CrossRef

54. Afonine, P. V., Grosse-Kunstleve, R. W., Echols, N., Headd, J. J., Moriarty, N. W., Mustyakimov, M., Terwilliger, T. C., Urzhumtsev, A., Zwart, P. H., and Adams, P. D. (2012) Towards automated crystallographic structure refinement with phenix.refine. *Acta Crystallogr. D Biol. Crystallogr.* **68,** 352–367 CrossRef

55. Schrodinger, LLC (2015) *The PyMOL Molecular Graphics System*, version 1.8, Schrodinger, LLC, New York

56. Schindelin, J., Arganda-Carreras, I., Frise, E., Kaynig, V., Longair, M., Pietzsch, T., Preibisch, S., Rueden, C., Saalfeld, S., Schmid, B., Tinevez, J. Y., White, D. J., Hartenstein, V., Eliceiri, K., Tomancak, P., and Cardona, A. (2012) Fiji: an open-source platform for biological-image analysis. *Nat. Methods* **9,** 676–682 CrossRef Medline

57. McWilliam, H., Li, W., Uludag, M., Squizzato, S., Park, Y. M., Buso, N., Cowley, A. P., and Lopez, R. (2013) Analysis Tool Web Services from the EMBL-EBI. *Nucleic Acids Res.* **41,** W597–W600 CrossRef Medline

58. Schrödinger Suite 2018–4 Protein Preparation Wizard (2016) Epik, Schrödinger, LLC; Impact (2018), Prime, Schrödinger, LLC, New York

59. Case, D. A., Babin, V., Berryman, J. T., Betz, R. M., Cai, Q., Cerutti, D. S., Cheatham, T. E., Darden, T. A., Duke, R. E., Gohlke, H., Goetz, A. W., Gusarov, S., Homeyer, N., Janowski, P., Kaus, J., *et al.* (2014) *AMBER 14,* University of California, San Francisco

60. Pettersen, E. F., Goddard, T. D., Huang, C. C., Couch, G. S., Greenblatt, D. M., Meng, E. C., and Ferrin, T. E. (2004) UCSF Chimera: a visualization system for exploratory research and analysis. *J. Comp. Chem.* **25,** 1605–1612 CrossRef Medline

61. Homeyer, N., and Gohlke, H. (2012) Free energy calculations by the molecular mechanics Poisson-Boltzmann surface area method. *Mol. Inform.* **31,** 114–122 CrossRef Medline

62. Cau, Y., Fiorillo, A., Mori, M., Ilari, A., Botta, M., and Lalle, M. (2015) Molecular dynamics simulations and structural analysis of *Giardia duodenalis* 14-3-3 protein-protein interactions. *J. Chem. Inf. Model.* **55,** 2611–2622 CrossRef Medline

63. Poli, G., Lapillo, M., Granchi, C., Caciolla, J., Mouawad, N., Caligiuri, I., Rizzolio, F., Langer, T., Minutolo, F., and Tuccinardi, T. (2018) Binding investigation and preliminary optimisation of the 3-amino-1,2,4-triazin-5(2H)-one core for the development of new Fyn inhibitors. *J. Enzyme Inhib. Med. Chem.* **33,** 956–961 CrossRef Medline

64. Naïm, M., Bhat, S., Rankin, K. N., Dennis, S., Chowdhury, S. F., Siddiqi, I., Drabik, P., Sulea, T., Bayly, C. I., Jakalian, A., and Purisima, E. O. (2007) Solvated interaction energy (SIE) for scoring protein-ligand binding affinities: 1. exploring the parameter space. *J. Chem. Infor. Model.* **47,** 122–133 CrossRef Medline

65. Mamonova, T., Kurnikova, M., and Friedman, P. A. (2012) Structural basis for NHERF1 PDZ domain binding. *Biochemistry* **51,** 3110–3120 CrossRef Medline

ASBMB